JOURNAL OF THERMOPHYSICS AND HEAT TRANSFER
Vol. 18, No. 3, July–September 2004

Hydrodynamic and Thermal Study of a Water-Filled Micro-Heat-Pipe Array

Stéphane Launay,* Valérie Sartre,† and Monique Lallemand‡
Institut National des Sciences Appliquées, 69621 Villeurbanne Cedex, France

A detailed mathematical model for predicting the heat transport capability and the temperature distribution along the axial direction of a 55-micro-heat-pipe array, filled with a polar fluid (water), has been developed. This steady-state model combines hydrodynamic flow equations with heat transfer equations in both the condensing and evaporating thin films. The velocity, pressure, and temperature distributions in the vapor and liquid phases are calculated. Various boundary conditions fixed to the micro-heat-pipe evaporator and condenser have been simulated to study the thermal performance of the micro-heat-pipe array below and above the capillary limit. The effect of the dryout or flooding phenomena on the micro-heat-pipe performance, according to boundary conditions and fluid fill charge, can also be predicted.

Nomenclature

A	=	cross-sectional area, m^2
g	=	gravitational acceleration, m/s^2
H	=	height, m
h	=	heat transfer coefficient, $W/m^2 \cdot K$
h_{lv}	=	latent heat of vaporization, J/kg
K	=	curvature, m^{-1}
L	=	axial length, m
l	=	wall wetted width, m
$\bar{M}$	=	molar weight, kg/mol
m	=	mass, kg
$\dot{m}_e$	=	evaporating mass transfer rate, kg/s
n	=	number of control volumes
P	=	pressure, Pa
p	=	perimeter, m
q	=	heat flux, W/m^2
Q	=	heat transfer rate, W
R_{th}	=	thermal resistance, K/W
$\bar{R}$	=	gas constant, $J/mol \cdot K$
r_c	=	meniscus curvature radius, m
T	=	temperature, K or °C
u	=	velocity, m/s
$\bar{V}$	=	molar volume, m^3/mol
W	=	width, m
z	=	axial coordinate, m
α	=	contact angle, deg
δ	=	thickness, m
δ'	=	film slope
η	=	coordinate, m
θ	=	micro-heat-pipe tilt angle, deg
λ	=	thermal conductivity, $W/m \cdot K$
λ^*	=	thermal conductivity ratio
μ	=	viscosity, kg/m s
ξ	=	coordinate, m
ρ	=	density, kg/m^3
σ	=	surface tension, N/m
τ	=	shear stress, Pa

Subscripts

A	=	adiabatic
ad	=	adhesion
C	=	condenser
E	=	evaporator
eff	=	effective
ext	=	external
i	=	interfacial
l	=	liquid
max	=	maximum
sat	=	saturation
T	=	total
v	=	vapor
w	=	wall
0	=	at $\xi = 0$

Received 28 October 2002; accepted for publication 29 September 2003.

*Postdoctoral Fellow, Centre de Thermique, Unité Mixte de Recherche Centre National de la Recherche Scientifique 5008, Institut National des Sciences Appliquées, 20 Av. A. Einstein; launay@cethil.insa-lyon.fr.

†Assistant Professor, Centre de Thermique, Unité Mixte de Recherche Centre National de la Recherche Scientifique 5008, Institut National des Sciences Appliquées, 20 Av. A. Einstein; sartre@cethil.insa-lyon.fr.

‡Professor, Centre de Thermique, Unité Mixte de Recherche Centre National de la Recherche Scientifique 5008, Institut National des Sciences Appliquées, 20 Av. A. Einstein; m.lal@cethil.insa-lyon.fr.

I. Introduction

MICRO heat pipes (MHP) are commonly used as efficient heat spreaders to eliminate hot spots and to reduce temperature gradients of electronic equipment. A MHP consists of a small noncircular channel that uses sharp-angled corners for the capillary pumping. To predict the MHP performance, many theoretical models, based on vapor and liquid flows along the MHP, have been developed.[1,2] However, previous investigations on evaporating extended meniscis in grooves of various geometries have shown that models based on the fundamental laws of physics should correctly predict the real system behavior only if the microregion is considered.[3] Indeed, in this region, the liquid film thickness is so small that the intermolecular forces become important. Depending on the fluid polarity, the short-range attractive forces between the liquid and the wall molecules are quite different and then affect the apparent contact angle of the liquid on the wall.[4] For strong polar working fluids, the intermolecular forces are composed of molecular and electrostatic interactions. These forces produce an adhesion pressure in the liquid, which causes the liquid to spread out over the wall. Varying the adhesion forces results in a noticeable change in the meniscus profile.[5] The effect of these forces on the temperature difference between the saturated vapor and the meniscus interface has been investigated by Stephan and Büsse[6] and Hallinan and Chebaro.[7] In previous work,[8] an MHP model taking into account the microregion has been coupled to a capillary flow model to calculate

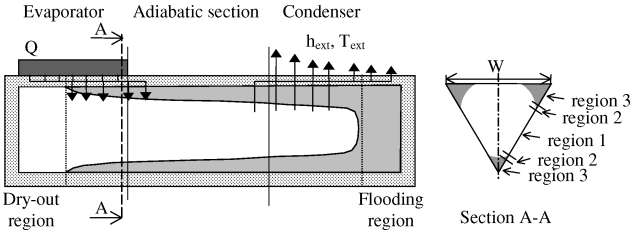

Fig. 1 Schematic diagram of the MHP.

the local heat transfer coefficients in an aluminium/ammonia MHP evaporator. Various studies have been conducted to determine the thermal performance of an MHP. Mallik et al.[9] and Huang et al.[10] have developed three-dimensional conduction models, with the assumption of an anisotropic conductivity of the material to determine potential advantages of integrating an array of very small heat pipes in the substrate of semi conductor chips. Another way to determine the longitudinal temperature variation, to solve the liquid and vapour phase energy equations for the evaporator and the condenser sections, has been used by Wu and Peterson[11] and Sobhan et al.[12]

In the present work, triangular MHPs, filled with water, are studied (Fig. 1). One of the particularities of the model is to study the MHP thermal performance vs the fluid fill charge. The liquid distribution and the temperature profiles are determined from the model, where heat transfer and fluid flow models in microscopic and macroscopic regions are coupled. The microscopic analysis allows the determination of the heat flux profile and the thermal resistance in each section of the condenser and the evaporator from the liquid film thickness. Thus, flooding and/or dryout lengths, reducing the MHP effective thermal conductivity, are calculated for each MHP extremity, respectively, vs the fluid fill charge and the heat input.

II. Modeling

A. Fluid Flows Along the MHP

Liquid and vapor flows have been investigated in a water MHP, whose cross section is an isosceles triangle. Its apex angle (70 deg) is fixed by the silicon MHP fabrication technique using an anisotropic etching with potassium hydroxide. During operation, the working fluid recedes into the MHP corners, generating the necessary capillary forces to drive the condensate back to the evaporator. By differentiating the Laplace–Young equation with respect to the longitudinal MHP coordinate z and neglecting some terms (Marangoni effect, etc.) as many authors have done,[1,13] we have

$$\frac{\mathrm{d}P_l}{\mathrm{d}z} = \frac{\mathrm{d}P_v}{\mathrm{d}z} - \frac{\mathrm{d}}{\mathrm{d}z}\left(\frac{\sigma}{r_c}\right) \tag{1}$$

To formulate the differential equations governing the flows inside the MHP, the following assumptions are made: 1) there are steady-state conditions, 2) in each MHP cross section, the vapor properties are assumed constant but variable along the MHP axial direction, 3) both liquid and vapor flows are laminar and incompressible, 4) the interfacial curvature, in the axial direction of the MHP, is neglected, 5) the wall temperature T_w in each section of the MHP is constant, 6) the heat flux Q_E is uniformly distributed along the axial evaporator length L_E but varies along the MHP perimeter, and 7) axial heat conduction is neglected if there is no dryout or flooding zone.

The fluid flow model is based on a one-dimensional model developed by Launay et al.[14] and Zaghdoudi et al.[15] The MHP is divided into several control volumes for which the mass, momentum, and energy equations are written for the liquid and vapor phases. For the energy equation, heat is supposed to be transferred by vaporization and the liquid–vapor interface is at the thermal equilibrium state. The numerical model is developed considering the counter current flows of vapor and liquid in the microchannel. The liquid and vapor cross-sectional areas A_l and A_v, the wetted perimeters p_{lw} and p_{vw}, and the liquid–vapor interfacial perimeter p_i are all expressed in terms of r_c, of the control volume length $\mathrm{d}z$, and the geometrical characteristics. These conservation equations can be written as

$$\rho_v \frac{\mathrm{d}(A_v u_v)}{\mathrm{d}z} = -A_i \rho_l u_i \tag{2}$$

$$\frac{\mathrm{d}(A_l u_l)}{\mathrm{d}z} = A_i u_i \tag{3}$$

$$\rho_v \frac{\mathrm{d}(A_l u_l)}{\mathrm{d}z} = -\frac{\mathrm{d}(A_v P_v)}{\mathrm{d}z} - |\tau_i| p_i - |\tau_{vw}| p_{vw} - \rho_v A_v g \sin\theta \tag{4}$$

$$\rho_l \frac{\mathrm{d}\left(A_l u_l^2\right)}{\mathrm{d}z} = -\frac{\mathrm{d}(A_l P_l)}{\mathrm{d}z} + |\tau_i| p_i + |\tau_{lw}| p_{lw} - \rho_l A_l g \sin\theta \tag{5}$$

where $u_i = -Q_E / L_E \rho_l A_i h_{\mathrm{lv}}$ is the radial phase change velocity. The shear stresses τ are determined according to the Longtin et al. expression.[1]

Equations (1–5) constitute a set of five first-order, nonlinear, coupled ordinary differential equations with five unknown variables: r_c, u_l, u_v, P_l, and P_v. This system is solved numerically with the following boundary conditions:

$$r_c|_{z=L_T} = r_{c,\max}, \qquad u_l|_{z=L_T} = u_v|_{z=L_T} = 0$$

$$P_v|_{z=L_T} = P_{\mathrm{sat}}, \qquad P_l|_{z=L_T} = P_{\mathrm{sat}} - \sigma / r_{c,\max}$$

The maximum curvature radius $r_{c,\max}$, located at the condenser end, is the radius of the inscribed circle in the inner triangular cross section. Solving the differential equation system from the end of the condenser allows the prediction of hydrodynamic and thermal characteristics of the MHP whatever the fluid fill charge and the boundary conditions fixed at the evaporator and condenser sections.

B. Governing Equations of Heat Transfer

The mathematical model of the evaporating and condensing regions allows the determination of the temperature distribution along the axial direction. This approach includes the effects of the capillary-induced flow in the corners and the flow and the evaporation of the thin-film caused by the adhesion pressure P_{ad} and the surface tension in the thin film region. In the heat transfer model of each MHP control volume $[(A_l + A_v)\,\mathrm{d}z]$, the thermal resistance R_{th} depends on the liquid film thickness, normal to the interface, calculated with the evaporator and condenser models,

$$\frac{1}{R_{\mathrm{th}}} = \sum_{j=1}^{n} \frac{1}{R_{\mathrm{th},j}} = \sum_{j=1}^{n} \frac{\lambda_l \cos\alpha_j}{\delta_j}\,\mathrm{d}z\,\mathrm{d}\xi \tag{6}$$

where ξ is the coordinate along the triangle perimeter divided into n elementary lengths $\mathrm{d}\xi$ and the local contact angle α_j is deduced from the film thickness gradient.

1. *Heat Transfer in the Evaporator*

As shown in Fig. 2, the liquid–vapor interface, when it is close to the wall, is composed of three regions: 1) the adsorbed film region, where this film cannot be evaporated due to the high adhesion forces; 2) the evaporating thin film region, so-called microregion, where a great part of evaporation occurs; and 3) the macrofilm, where the adhesion forces are negligible and the meniscus curvature radius is constant.

In the evaporating thin film region, the high evaporation rate induces a transverse liquid flow, which is governed by the surface tension and the adhesion forces. The second mechanism is dominating when the meniscus is very close to the wall. The capillary pressure P_c is then given by

$$P_c = P_v - P_l = \sigma K - P_{\mathrm{ad}} \tag{7}$$

The term σK accounts for the meniscus curvature K, which is linked to the film thickness δ_j by

$$K = \frac{\mathrm{d}^2\delta_j}{\mathrm{d}\xi^2}\left[1 + \left(\frac{\mathrm{d}\delta_j}{\mathrm{d}\xi}\right)^2\right]^{-\frac{3}{2}} \tag{8}$$

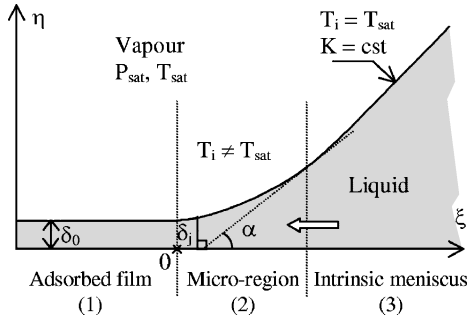

Fig. 2 Cross section of the liquid film in the evaporator section.

For water, which is a strong polar working fluid, P_{ad} depends on δ_j by a logarithmic relation,[16]

$$P_{ad} = \rho_l(\bar{R}/\bar{M})T_i \ln\left[A_l(\delta_j/3.3)^{B_l}\right] \quad \text{for} \quad \delta_j \le 3.3/A_l^{1/B_l}$$
$$P_{ad} = 0 \quad \text{for} \quad \delta_j > 3.3/A_l^{1/B_l} \tag{9}$$

A_l and B_l are constants, which only depend on the fluid nature. For water, $B_l = 0.0243$ and $A_l = 1.5336$ (SI unit). The evaporation rate is calculated from the Wayner et al. model.[17] From the mass and momentum equations for the transverse liquid flow, the evaporating mass flux is

$$\dot{m}_e = \frac{\rho_l}{3\mu_l}\frac{\mathrm{d}}{\mathrm{d}\xi}\left(\delta_j^3\frac{\mathrm{d}P_c}{\mathrm{d}\xi}\right) \tag{10}$$

Both the adhesion and surface tension forces reduce the liquid evaporation and lead to an increase of the interfacial temperature. Thus, the equilibrium interface temperature T_i is higher than the saturation temperature T_{sat}. At steady state, the heat conduction of liquid film is equal to the evaporation heat; thus, T_i is

$$T_i = \frac{T_w\lambda_l/(\delta_j h_{lv}) + aT_v + b\sigma K}{a + b\rho_l(\bar{R}/\bar{M})\ln\left[A_l(\delta_j/\delta_j 3.3)^{B_l}\right] + \lambda_l/(\delta_j h_{lv})} \tag{11}$$

with

$$a = C_1\sqrt{\bar{M}/2\pi\bar{R}T_i}(P_v\bar{M}h_{lv}/\bar{R}T_vT_i)$$
$$b = C_1\sqrt{\bar{M}/2\pi\bar{R}T_i}(\bar{V}_lP_v/\bar{R}T_i)$$

where C_1 is the evaporation coefficient equal to 2 (Ref. 7).

The model output parameters are the interfacial temperature T_i, the radial heat flux distribution along the wall q, and the film thickness δ_j from which is deduced its slope δ_j' and the interface curvature K. The total heat flux dissipated in the microregion and the contact angle can be predicted, too. The origin of ξ is set at the intersection of the adsorbed thin film region and the evaporating interfacial region. The boundary conditions corresponding to the set of Eqs. (7–11) at $\xi = 0$ can be expressed as

$$\delta_0 = 3.3\left\{\frac{1}{A_l}\exp\left[-\frac{a(T_w - T_v)}{b\rho_l(\bar{R}/\bar{M})T_w}\right]\right\}^{1/B_l}$$
$$K_0 = 0, \qquad \delta_0' = 0, \qquad Q_0 = 0, \qquad T_{i0} = T_w$$

where δ_0 is the thickness of the adsorbed thin film.

The heat transfer coefficient of the macrofilm is calculated from the liquid film thickness. In this region, the interfacial temperature T_i is supposed equal to the saturation temperature.

In an operating MHP, vaporization can also take place in the adiabatic section, particularly when dryout occurs at the end of the evaporator.[3] Thus, the microregion model is applied until T_w is greater than T_{sat}. If the dryout occurs, the longitudinal conduction thermal resistance into the wall is taken into account.

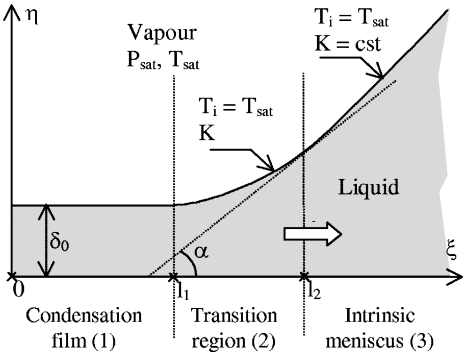

Fig. 3 Cross section of the liquid film in the condenser section.

2. Heat Transfer in the Condenser

At the condenser, the liquid is assumed to flow transversally toward the corners and then axially in the meniscus region. The condensing film is divided into three regions (Fig. 3): 1) a film region of constant thickness, 2) a transition region where both the film thickness and the curvature vary, and 3) a meniscus region of constant curvature. In region 1, the film thickness is calculated by the Nusselt theory, in which the driving forces are the capillary forces,

$$\delta(\xi) = \left[\frac{4\mu_l\lambda_l(T_{sat} - T_w)\,\xi}{\rho_l(\mathrm{d}P/\mathrm{d}\xi)\,h_{lv}}\right]^{\frac{1}{4}} \tag{12}$$

with $\mathrm{d}P/\mathrm{d}\xi = (\mathrm{d}/\mathrm{d}\xi)(\sigma/r_c)$.

In the transition region, the film profile is calculated from a fourth-order polynomial, whose coefficients are defined according to the boundary conditions

$$\left.\frac{\mathrm{d}\delta}{\mathrm{d}\xi}\right|_{\xi=l_1} = 0, \qquad \left.\frac{\mathrm{d}\delta}{\mathrm{d}\xi}\right|_{\xi=l_2} = \tan\alpha$$
$$\left.\frac{\mathrm{d}^2\delta}{\mathrm{d}\xi^2}\right|_{\xi=l_2} = \frac{1}{r_c}, \qquad \left.\frac{\mathrm{d}^3\delta}{\mathrm{d}\xi^3}\right|_{\xi=l_1} = 0$$

where α is the apparent contact angle of the fluid and r_c is the constant curvature radius of the meniscus region. At the condenser, the origin of ξ is set at the middle of one side of the channel. Then, the width of the regions 1, 2, and 3 are $l_1, l_2 - l_1$, and $l_T - l_2$, respectively, with l_T corresponding to the total wetted width, equal to the triangle half-basis.

III. Numerical Treatment

To determine temperature and heat transfer rate distributions along the MHP, the models of fluid flows and heat transfer in the evaporator and condenser sections are coupled together and numerically solved for each control volume of length $\mathrm{d}z$. The fluid flow and microregion models are both solved using the fourth-order Runge–Kutta procedure. Thus, for each control volume, $\delta_j(\xi)$, A_l, A_v, and R_{th}, the wall temperature T_w and then Q can be determined by the condenser and evaporator heat transfer models, by use of the capillary radius r_c calculated by the fluid flow model. The numerical treatment scheme, developed by Launay[14] can be summarized as follows. The input data are the heat load at the evaporator Q_T, the MHP array fluid fill charge, and the external wall temperature at the condenser section. T_{sat} and r_c are first initialized at the end of the condenser, $z = L_T$. The heat transfer rate dissipated in a given control volume, calculated by the condenser heat transfer model, is then introduced as input data of the fluid flow model. Then r_c, P_l, P_v, u_l, and u_v are calculated for the next control volume, and this procedure is repeated. Comparing the total heat flux dissipated at the condenser with the heat transfer rate input allows us to determine T_{sat} iteratively. At the evaporator section, the wall temperature of the evaporator end, $z = L_E$, is first initialized and then corrected until the whole heat load, dissipated along the evaporator, is equal to the

heat input Q_T. The fluid mass is deduced from the cross-sectional area of each phase along the MHP. To obtain equality between calculated and input fluid fill charges, the maximum curvature radius at the end of the condenser, $z = L_T$, or the flooding zone length are adjusted.

IV. Results and Discussion

The dimensions of the 55-MHP array are the following (Fig. 1): triangle basis $W = 230$ μm, triangle height $H = 165$ μm, total length $L_T = 20$ mm, evaporator and adiabatic section lengths $L_E = L_A = 5$ mm, and condenser length $L_C = 10$ mm. The working fluid is pure saturated water, and the walls are made of silicon.

First, results about meniscus curvature radius, velocity, pressure, and temperature distributions in the vapor and liquid phases are presented with respect to heat inputs at the evaporator. Then, the heat flux and film thickness distributions in a cross section of the evaporator and the condenser are given. The effect of the fluid fill charge and the MHP internal width on the MHP performance are also studied.

A. Capillary Limit and Optimum Fill Charge

The capillary limit, which corresponds to the maximum heat transfer capability, without dryout at the evaporator and without flooding at the condenser, is reached when the capillary radius r_c is as small as possible at $z = 0$ and $r_c = r_{c,\max}$ at $z = L_T$. In these conditions, the fill charge is considered as an optimum. That r_c is as small as possible signifies that r_c would be negative for a next step on z. The r_c value depends on the dz value; it becomes smaller as dz decreases. For example, for dz equal to 20 μm, r_c minimum is equal to 4.5 μm for the capillary limit.

For the MHP array just described and with the following external conditions imposed at the condenser section, $T_{\text{ext}} = 50°\text{C}$ and $h_{\text{ext}} = 1000\ \text{W/m}^2 \cdot \text{K}$, the capillary limit is 2 W and the corresponding optimum fill charge is 3.6 mg. In the next simulations, the heat inputs correspond to the capillary limit and to a heat input slightly lower than this limit.

B. Liquid and Vapor Velocities Profiles

Vapor and liquid velocities in a MHP are mostly determined by the mass transfer due to the phase change and by the cross-sectional area of the vapor and the liquid. The liquid velocity profiles for heat inputs of 1.5, 1.9, and 2 W are shown vs z^* (the non-dimensional length z/L_T) in Fig. 4. Because the heat flux is supposed uniformly distributed along the axial evaporator length, the evaporating mass flow rate is constant in each section, and then, the total liquid mass flow rate increases linearly with z in the evaporator region. For $Q = 1.9$ W, by the consideration of the liquid flow direction (decreasing z), the liquid velocity increases from the condenser to a maximum at $z^* \approx 0.18$. Then, for $z^* < 0.18$, the liquid mass flow rate variation being greater than the liquid cross-sectional area variation, the liquid velocity decreases. For $Q = 2$ W (capillary limit), the maximum liquid velocity is reached when $z^* \to 0$. At the evaporator beginning, the strong increase of the liquid velocity is due to the strong decrease of the liquid cross-sectional area, which tends to zero. For a heat input greater than 2 W, dryout occurs. The vapor velocity profiles for 1.9 and 2 W are shown in Fig. 5. No significant differences are observed between these two heat input values. At the evaporator, the vapor production due to liquid evaporation leads to a vapor velocity increase beyond the beginning of the adiabatic section because of the axial heat conduction in the wall. In the adiabatic section, the vapor velocity still increases because of the decreasing vapor cross-sectional area until condensation occurs. Then, the vapor velocity decreases to zero. For the same reason, a vapor velocity decrease is observed before the limit between the condenser and adiabatic sections.

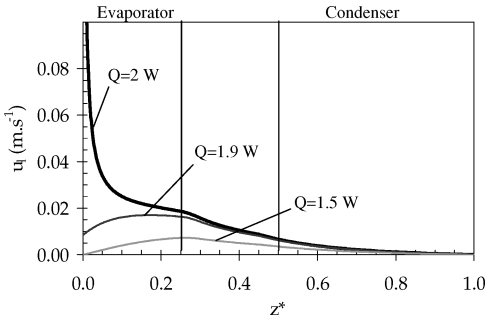

Fig. 4 Liquid velocity profiles for $Q = 1.5$, $Q = 1.9$, and $Q = 2$ W.

C. Pressure and Meniscus Curvature Radius Profiles

The liquid and vapor pressure profiles along the MHP for 1.5, 1.9, and 2 W are shown in Fig. 6. For 2 W, the vapor pressure drops along the MHP are weak as compared to the liquid ones. When the liquid pressure profiles are compared with the liquid velocity distributions (Fig. 4), the great decrease of the liquid pressure corresponds to the steep increase of the liquid velocity at the evaporator. At the same location, the liquid recession in the corners due to liquid evaporation is intensified by the great difference between liquid and vapor pressures. The meniscus curvature radius (Fig. 7) and, consequently, the liquid cross-sectional area, which is proportional to the square of the meniscus curvature radius,[18] decrease drastically.

The comparison of the velocity and pressure profiles of the liquid and the vapor for two close values of the heat input shows that the

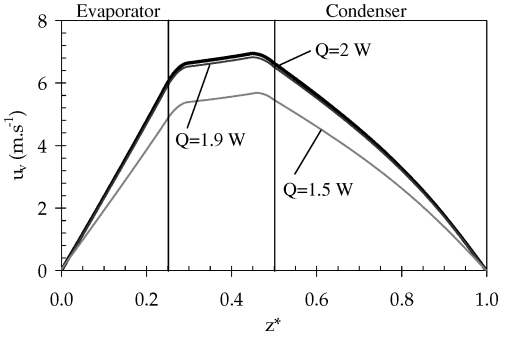

Fig. 5 Vapor velocity profiles for $Q = 1.5$, $Q = 1.9$, and $Q = 2$ W.

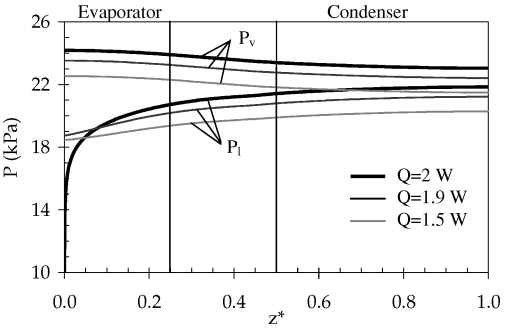

Fig. 6 Liquid and vapor pressures for $Q = 1.5$, $Q = 1.9$, and $Q = 2$ W.

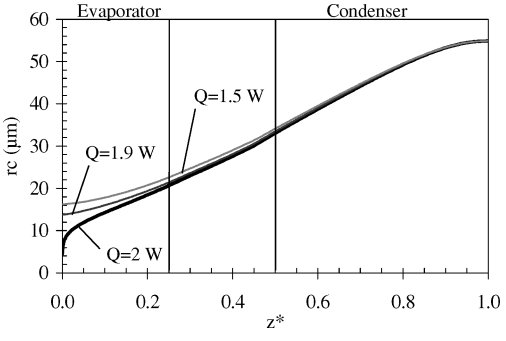

Fig. 7 Meniscus curvature radius for $Q = 1.5$, $Q = 1.9$, and $Q = 2$ W.

capillary pumping of the MHP is mainly limited by the liquid flow characteristics.

D. Saturation and Wall Temperature Profiles

The saturation temperature T_{sat} and the wall temperature T_w profiles are shown in Fig. 8 for 1.5, 1.9, and 2 W. T_{sat} is derived from the vapor pressure value, which is given by the fluid flow model, by assuming a liquid–vapor equilibrium state. T_w is deduced from T_{sat} and the liquid thermal resistance. Note, for each heat input, that the gradient along the MHP in the vapor phase is larger than the temperature gradients in the liquid film at the evaporator and the condenser sections. The temperature difference $|T_{sat} - T_w|$ is smaller at the condenser compared to the evaporator. This can be explained by a greater heat transfer area in the condenser section than in the evaporator. The temperature profiles for 1.9 and 2 W are quite similar with a 0.6-K gap. Indeed, the small heat input difference (0.1 W) is not sufficient to modify the liquid distribution along the MHP and to increase significantly the vapor pressure drops.

E. Meniscus Profile and Heat Transfer Rate in a MHP Cross Section

The meniscus profiles and heat transfer rates in the evaporator and condenser sections are shown in Figs. 9 and 10. The width of the wetted wall of a half-corner in a given cross section of the evaporator

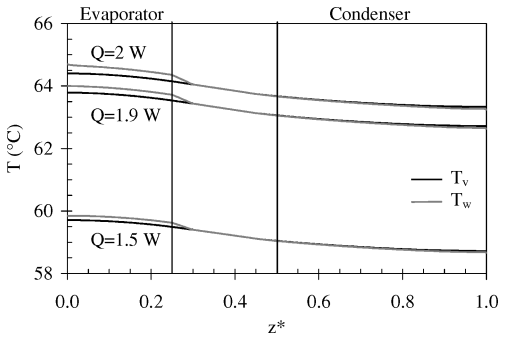

Fig. 8 Saturation and wall temperatures for $Q = 1.5$, $Q = 1.9$, and $Q = 2$ W.

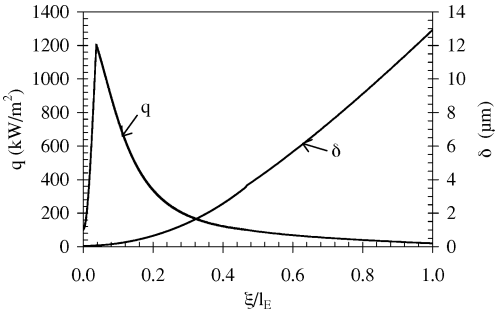

Fig. 9 Heat flux and film thickness variation in cross section of the evaporator.

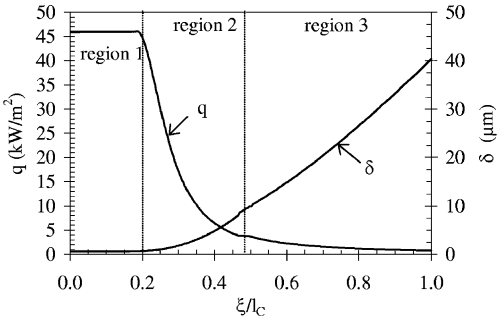

Fig. 10 Heat flux and film thickness variation in cross section of the condenser.

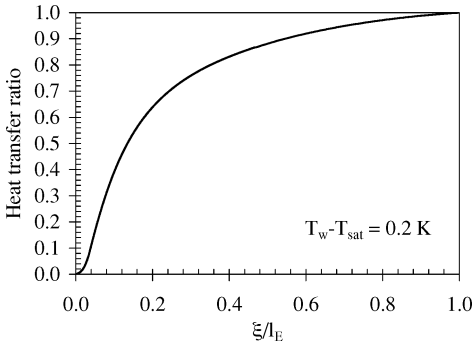

Fig. 11 Heat transfer ratio for a cross section of the evaporator.

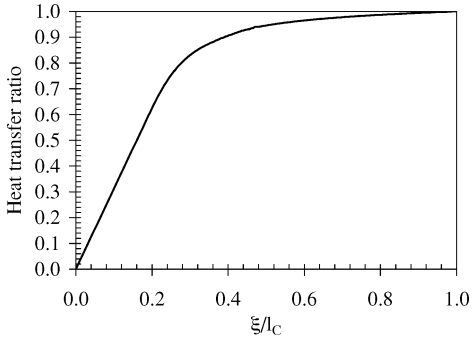

Fig. 12 Heat transfer ratio for a cross section of the condenser.

and the condenser are l_E and l_C, respectively. At the evaporator, as shown in Fig. 9, the heat transfer increases sharply at the transition of the adsorbed thin film region to the thin film evaporating region; then, it reaches a maximum ($q = 1.2\ 10^6$ W/m^2) in the microregion and decreases when the film thickness increases. In comparison, the heat transfer profile at the condenser (Fig. 10) is rather different: The heat transfer is constant at its highest value ($q = 4.6\ 10^4$ W/m^2) in the condensing region (region 1) and decreases when the film thickness increases. Figures 11 and 12 show quantitatively the heat transfer ratio dissipated by the evaporator and condenser sections. The heat transfer ratio is defined as

$$\text{heat transfer ratio} = \frac{\sum_{\xi=0}^{l} q\, d\xi\, dz}{Q_T\, dz/L_E \text{ or } L_C} \tag{13}$$

Note that 60% of the heat input ($Q_T\, dz/L_E$) is dissipated on 4 μm for a total wetted wall width $l_E = 23$ μm, in an evaporator cross section, and that 60% of the heat load ($\approx Q_T\, dz/L_C$) is dissipated on 15 μm for a total wetted wall width $l_C = 85$ μm, in a condenser cross section. Similiar to Peterson and Ma,[19] it can be concluded that the best way to increase the evaporating and condensing heat transfer is to increase the evaporating and condensing thin film regions by an enhanced geometry. These results have been also shown by Zaghdoudi et al.,[15] who compared the performance of a four-corner MHP with that of a three-corner MHP.

F. Effect of the Working Fluid Fill Charge

Simulations are made to study the effect of the fluid fill charge on the MHP array thermal performances. For $Q = 2$ W, the optimum fill charge for the MHP array, which is defined in Sec. IV. A, is equal to 3.6 mg and represents 18% of the MHP array volume.

In Fig. 13, λ^*_{eff}, which is the ratio between the effective thermal conductivity of the MHP array and the silicon thermal conductivity, is plotted vs the fluid fill charge for $Q = 2$ W. Ratio λ^*_{eff} reaches a maximum value for an amount of working fluid ($m \approx 4.4$ mg) slightly up to the optimum fill charge. For $m \approx 4.4$ mg, the flooding length at the end of the condenser is equal to 1.4 mm. The increase of λ^*_{eff} can be explained by the vapor thermal resistance reduction, which is more important than the increase of the liquid film thermal resistance at the condenser. The vapor thermal resistance reduction,

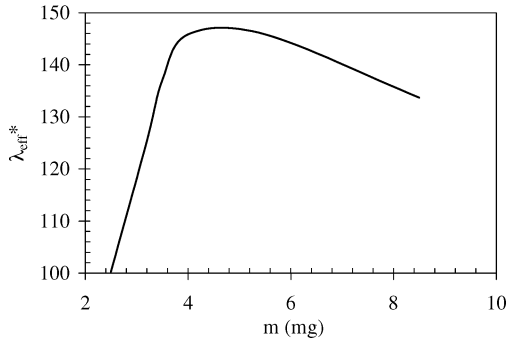

Fig. 13 Thermal conductivity ratio λ_{eff}^* vs the fluid fill charge, $Q = 2$ W.

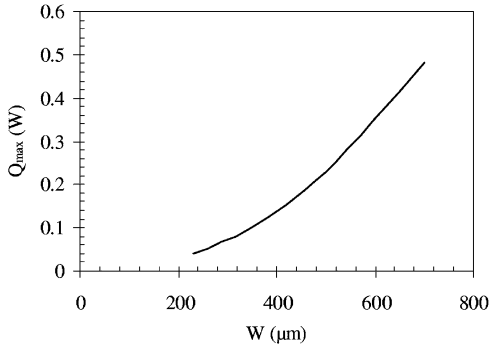

Fig. 14 Q_{max} along the MHP width.

calculated from the vapor pressure drops, is due to the reduction of the vapor flow length. Ratio λ_{eff}^* decreases when the increase of the liquid film thermal resistance at the condenser is no longer compensated by the vapor thermal resistance reduction along the MHP. Ratio λ_{eff}^* decreases drastically when the fill charge is lower than the optimum fill charge. Indeed, in these conditions, the maximum curvature radius at the end of the condenser is lower than the radius of the inscribed circle in the inner triangular cross section, and then, the liquid pressure drops become greater than the capillary pumping pressure: A dryout phenomenon occurs.

The behavior of a 3.6-mg charged MHP array has been investigated for heat inputs greater than 2 W. The effective thermal conductivity is almost constant when Q increases up to 30% of the capillary limit. In fact, in these conditions, only half of the evaporating region is dried, which is sufficient to dissipate Q without an important increase of the evaporator temperature.

G. Effect of the MHP Internal Width

In Fig. 14 the capillary limit Q_{max} as a function of the MHP width is shown. The MHP width W varies from 200 to 700 μm, with 700 μm being the largest width that can be realized in a 625-μm-thick silicon wafer. Q_{max} increases as the MHP width W increases because of the increase of A_l and A_v.

V. Conclusions

A numerical model has been developed to predict the fluid flows and heat transfer for an MHP array whose cross section is triangular. This study leads to a better understanding of the heat transfer distribution in the entire MHP. At the evaporator, heat is mainly transferred in the short thin film region, where the liquid is very close to the wall. It results from the effect of the adhesion forces on the meniscus curvature and from the capillary forces. Thus, to improve heat transfer, the microregion number in an MHP cross section must be as high as possible. For triangular MHPs, the heat transfer rate is rather limited by the large liquid pressure drops in the corners; nevertheless, the vapor pressure drops are not negligible. The thermal resistance of the vapor phase, calculated by considering the saturation conditions in each section of the MHP, is more important than the transversal thermal resistance in the liquid film and the wall. Thus, increasing the triangular MHP cross-section allows the increase of the liquid and vapor flow cross sections and consequently the increase of the capillary limit and the reduction of the vapor thermal resistance. It results an increase of the effective thermal conductivity of the MHP. The thermal performances of the MHP array are strongly dependent on the amount of working fluid: A too large amount leads to condenser flooding, and a too small amount leads to evaporator dryout. In both cases, the heat transfer areas are reduced, and the liquid thermal resistance increases.

References

[1]Longtin, J. P., Badran, B., and Gerner, F. M., "A One-Dimensional Model of a Micro Heat Pipe During Steady-State Operation," *Journal of Heat Transfer*, Vol. 116, Aug. 1994, pp. 709–715.

[2]Ma, H. B., and Peterson, G. P., "The Minimum Meniscus Radius and Capillary Heat Transport Limit in Micro Heat Pipes," *Journal of Heat Transfer*, Vol. 120, Feb. 1998, pp. 227–233.

[3]Ma, H. B., and Peterson, G. P., "Temperature Variation and Heat Transfer in Triangular Grooves with an Evaporating Film," *Journal of Thermophysics and Heat Transfer*, Vol. 11, No 1, 1997, pp. 90–97.

[4]Wayner, P. C., "Effect of Interfacial Phenomena in the Interline Region on the Rewetting of a Hot Spot," *International Journal of Heat and Mass Transfer,* Vol. 22, 1979, pp. 1033–1040.

[5]Qu, W., and Ma, T., "Effects of the Polarity of Working Fluids on Vapour–Liquid Flow and Heat Transfer Characteristics in a Capillary," *Proceedings of the International Conference on Heat Transfer and Transport Phenomena in Microscale*, ENEA, Italy, 2000, pp. 196–203.

[6]Stephan, P. C., and Büsse, C. A., "Analysis of the Heat Transfer Coefficient of Grooved Heat Pipe Evaporator Walls," *International Journal of Heat and Mass Transfer*, Vol. 35, No 2, 1992, pp. 383–391.

[7]Hallinan, K. P., and Chebaro, H. C., "Evaporation from an Extended Meniscus for Nonisothermal Interfacial Conditions," *Journal of Thermophysics and Heat Transfer*, Vol. 8, No. 4, 1994, pp. 709–716.

[8]Sartre, V., Zaghdoudi, M. C., and Lallemand, M., "Effect of Interfacial Phenomena on Evaporative Heat Transfer in Micro Heat Pipes," *International Journal of Thermal Science*, Vol. 39, No. 4, 2000, pp. 498–504.

[9]Mallik, A. K., Peterson, G. P., and Weichold, M. H., "On the Use of Micro Heat Pipes as an Integral Part of Semi Conductor Devices," *Journal of Electronic Packaging*, Vol. 114, No. 4, 1992, pp. 436–442.

[10]Huang, X. Y., Liu, C. Y., and Toh, K. C., "A Transient Three-Dimensional Model of Micro Heat Pipes Used as an Integral Part of Semi-Conductor Devices," *Microelectromechanical Systems (MEMS)*, American Society of Mechanical Engineers, Fairfield, NJ, Vol. 59, 1996, pp. 37–47.

[11]Wu, D., and Peterson, G. P., "Investigation of the Transient Characteristics of a Micro Heat Pipe," *Journal of Thermophysics*, Vol. 5, No. 2, 1991, pp. 129–134.

[12]Sobhan, C. B., Xiaoyang, H., and Yu, L. C., "Investigations on Transient and Steady-State Performance of a Micro Heat Pipe," *Journal of Thermophysics and Heat Transfer*, Vol. 14, No. 2, 2000, pp. 161–169.

[13]Khrustalev, D., and Faghri, A., "Thermal Analysis of a Micro Heat Pipe," *Journal of Heat Transfer*, Vol. 116, Feb. 1994, pp. 189–198.

[14]Launay, S., Sartre, V., and Lallemand, M., "Thermal Study of a Water-Filled Micro Heat Pipe Including Heat Transfer in Evaporating and Condensing Microfilms," *Proceedings of the 12th International Heat Transfer Conference*, 2002, Elsevier, New York, pp. 471–476.

[15]Zaghdoudi, M. C., Sartre, V., and Lallemand, M., "Theoretical Investigation of Micro Heat Pipes Performance," *Proceedings of the 10th International Heat Pipe Conference*, Inst. for Technology and Energy Systems, Univ. of Stuttgart, Stuttgart, Germany, 1997, p. 6.

[16]Holm, F. W., and Goplen, S. P., "Heat Transfer in the Meniscus Thin Film Transition Region," *Journal of Heat Transfer*, Vol. 101, Aug. 1979, pp. 543–547.

[17]Wayner, P. C., Kao, Y. K., and LaCroix, L. V., "The Interline Heat-Transfer Coefficient of an Evaporating Wetting Film," *International Journal of Heat and Mass Transfer*, Vol. 19, 1976, pp. 487–492.

[18]Ha, J. M., and Peterson, G. P., "The Heat Transport Capacity of Micro Heat Pipes," *Journal of Heat Transfer*, Vol. 120, Nov. 1998, pp. 1064–1071.

[19]Peterson, G. P., and Ma, H. B., "Temperature Response of Heat Transport in a Micro Heat Pipe," *Journal of Heat Transfer*, Vol. 121, May 1999, pp. 438–445.